Current Biology, Volume *31*

Supplemental Information

Plastin and spectrin cooperate to stabilize the actomyosin cortex during cytokinesis

Ana Filipa Sobral, Fung-Yi Chan, Michael J. Norman, Daniel S. Osório, Ana Beatriz Dias, Vanessa Ferreira, Daniel J. Barbosa, Dhanya Cheerambathur, Reto Gassmann, Julio Monti Belmonte, and Ana Xavier Carvalho

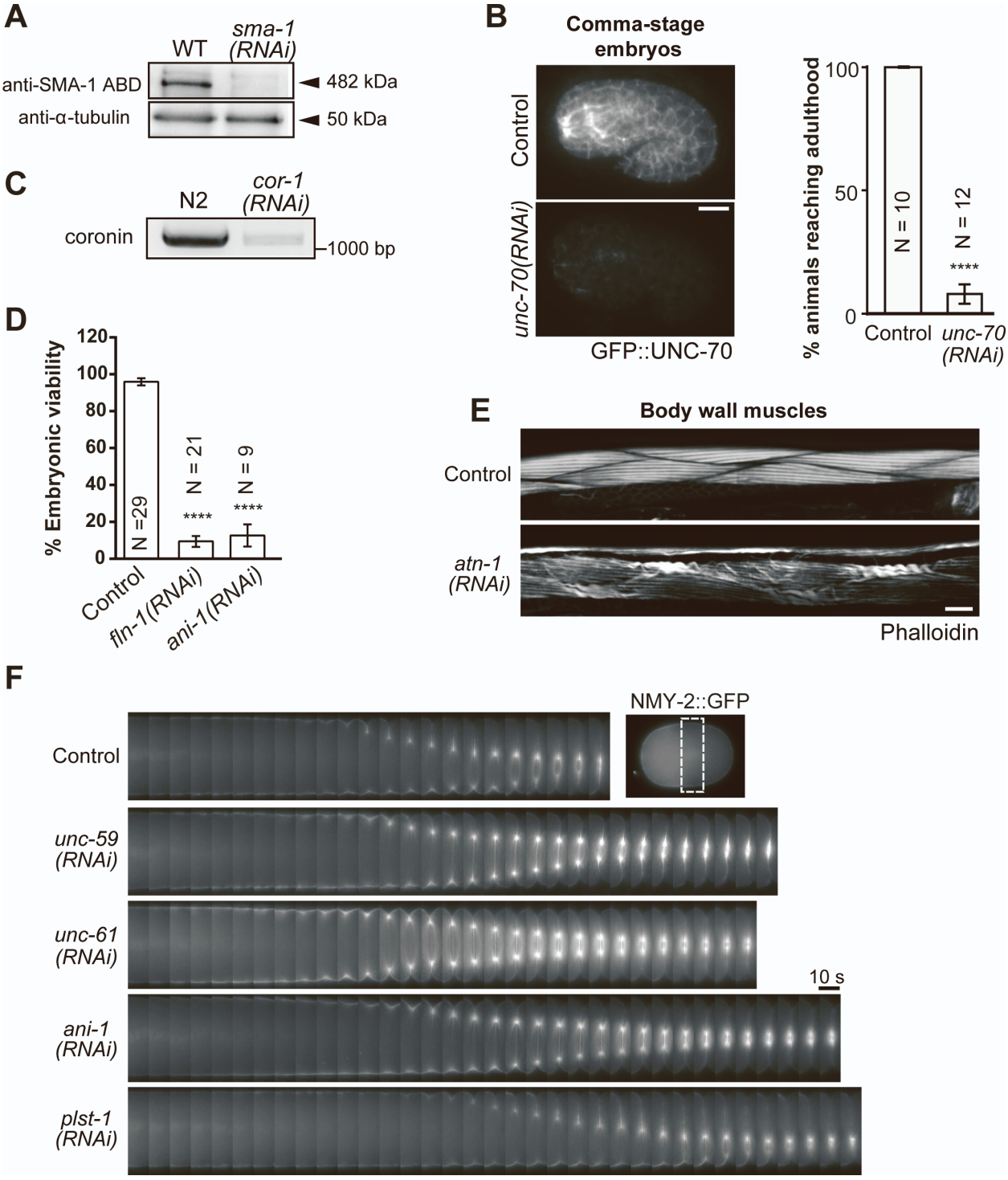
A
WT
sma-1 (RNAi)
anti-SMA-1 ABD
anti-α-tubulin
482 kDa
50 kDa
B
Comma-stage embryos
Control
unc-70(RNAi)
GFP::UNC-70
% animals reaching adulthood
100
50
0
N = 10
N = 12
****
Control
unc-70 (RNAi)
C
N2
cor-1 (RNAi)
coronin
1000 bp
D
% Embryonic viability
120
100
80
60
40
20
0
N =29
N = 21
N = 9
****
****
Control
fln-1(RNAi)
ani-1(RNAi)
E
Body wall muscles
Control
atn-1 (RNAi)
Phalloidin
F
NMY-2::GFP
Control
unc-59 (RNAi)
unc-61 (RNAi)
10 s
ani-1 (RNAi)
plst-1 (RNAi)

Figure S1. Validation of RNAi efficiency. Related to Figure 1.

(A) Immunoblot of adult *C. elegans* lysate with an antibody raised against the actin-binding domain (ABD) of SMA-1, showing efficient depletion of SMA-1 after *sma-1(RNAi)*. WT is wild-type. α-tubulin serves as the loading control. **(B)** *(left)* Stills of comma-stage embryos expressing endogenous UNC-70::GFP before and after *unc-70(RNAi)*. Scale bar, 10 μm. *(right)* Percentage (mean ± 95% CI) of *unc-70(RNAi)* animals that develop to adulthood. Most *unc-70(RNAi)* animals arrest at the L1 stage, consistent with a previous study [S1]. Statistical significance was determined using unpaired two-tailed Student t-test: $^{****}p \leq 0.0001$. **(C)** RT-PCR for *cor-1* in N2 controls and after *cor-1(RNAi)* using primers Fw 5'-CGTCGACAAGGACTATCCA-3' and Rv 5'-GGAGCCAAAGTGCTCAAA-3' that amplify the 3 isoforms. Method was described previously [S2]. **(D)** Percentage of embryonic viability (mean ± 95% CI) in N2 controls, after *fln-1(RNAi)*, and *ani-1(RNAi)*, consistent with previous studies [S3,S4]. Statistical significance was determined using one-way ANOVA followed by Dunnett's multiple comparison test: $^{****}p \leq 0.0001$. **(E)** Images of body wall muscles stained with phalloidin. *atn-1(RNAi)* results in curled F-actin fibers, as expected from previous study [S5]. Method was described previously [S6]. Scale bar, 10 µm. **(F)** Images of the equatorial region in dividing one-cell embryos expressing NMY-2::GFP. The first frame corresponds to anaphase onset. Symmetric furrow closure confirms efficient RNAi-mediated depletion of UNC-59, UNC-61 and ANI-1, as described previously [S7]. Prolonged cytokinesis confirms efficient RNAi-mediated depletion of PLST-1. Scale bar, 10 μm.

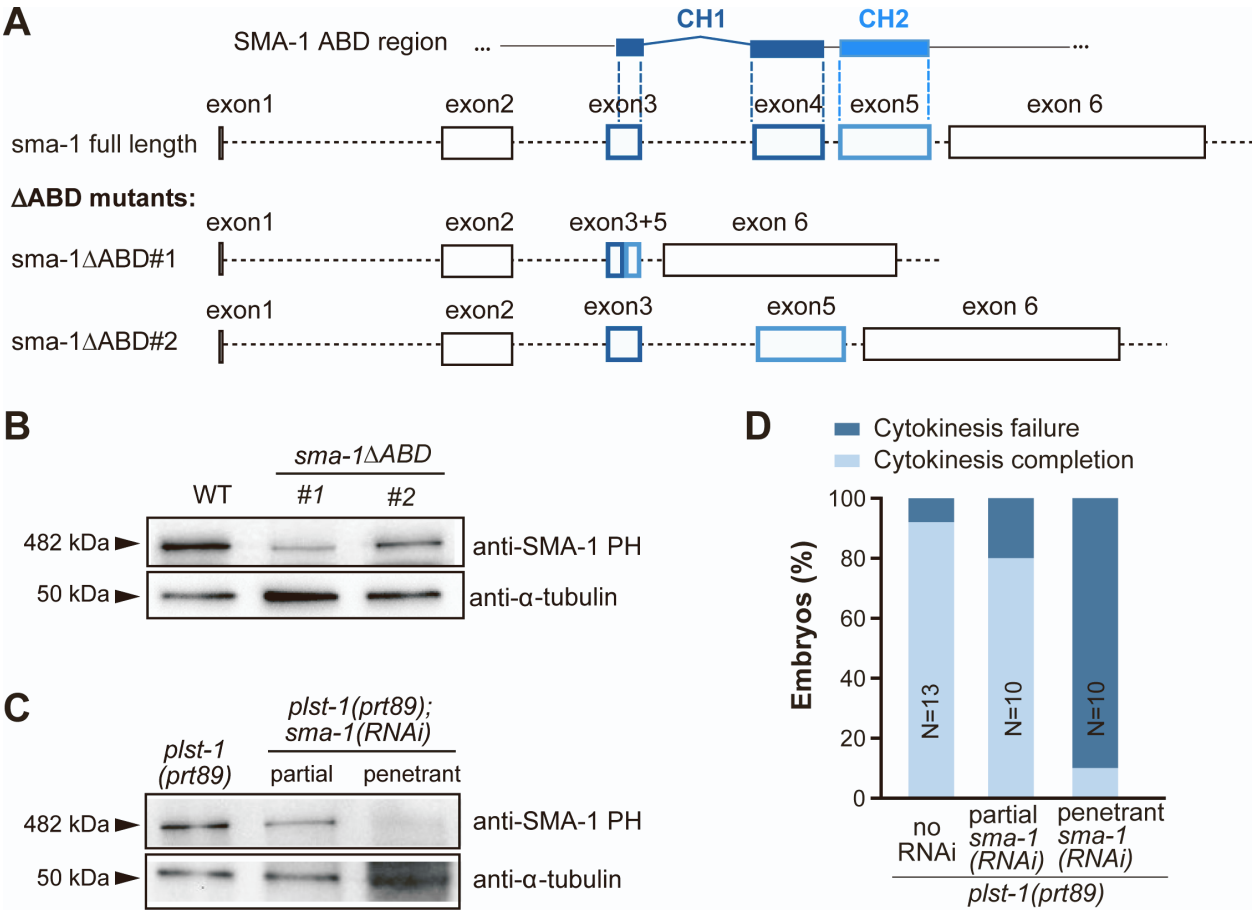
A
SMA-1 ABD region
CH1
CH2
exon1
exon2
exon3
exon4
exon5
exon 6
sma-1 full length
ΔABD mutants:
exon3+5
sma-1ΔABD#1
sma-1ΔABD#2
B
sma-1ΔABD
WT
#1
#2
482 kDa
50 kDa
anti-SMA-1 PH
anti-α-tubulin
C
plst-1(prt89); sma-1(RNAi)
plst-1 (prt89)
partial
penetrant
D
Cytokinesis failure
Cytokinesis completion
Embryos (%)
N=13
N=10
N=10
no RNAi
partial sma-1 (RNAi)
penetrant sma-1 (RNAi)
plst-1(prt89)

Figure S2. SMA-1 deletion mutants that lack most of the actin binding domain are expressed at lower levels but this is unlikely to explain the cytokinesis failure in the *plst-1(prt89)* background. Related to Figure 4.

(A) Schematic of the first 6 exons and 5 introns of the *sma-1* gene in wild-type and after editing to obtain ABD deletions (ΔABD). Part of exon 3 and exon 4 encode the first CH domain (CH1), and exon 5 encodes the second CH domain (CH2). SMA-1ΔABD#1 lacks most of exon 3, the entire exon 4, and most of exon 5. SMA-1ΔABD#2 lacks exon 4. **(B)** Immunoblot of adult *C. elegans* lysate with an affinity-purified anti-SMA-1 antibody raised against the PH domain, showing SMA-1 levels in animals expressing the two different SMA-1ΔABD versions. α-tubulin serves as the loading control. **(C)** Anti-SMA-1 immunoblot of adult *C. elegans* lysate, showing protein levels in *plst-1(prt89)* animals after partial or penetrant *sma-1(RNAi)*. α-tubulin serves as the loading control. (**D**) Percentage of cytokinesis completion/failure in one-cell *plst-1(prt89)* embryos after partial and penetrant depletion of SMA-1. N indicates the number of embryos analyzed.

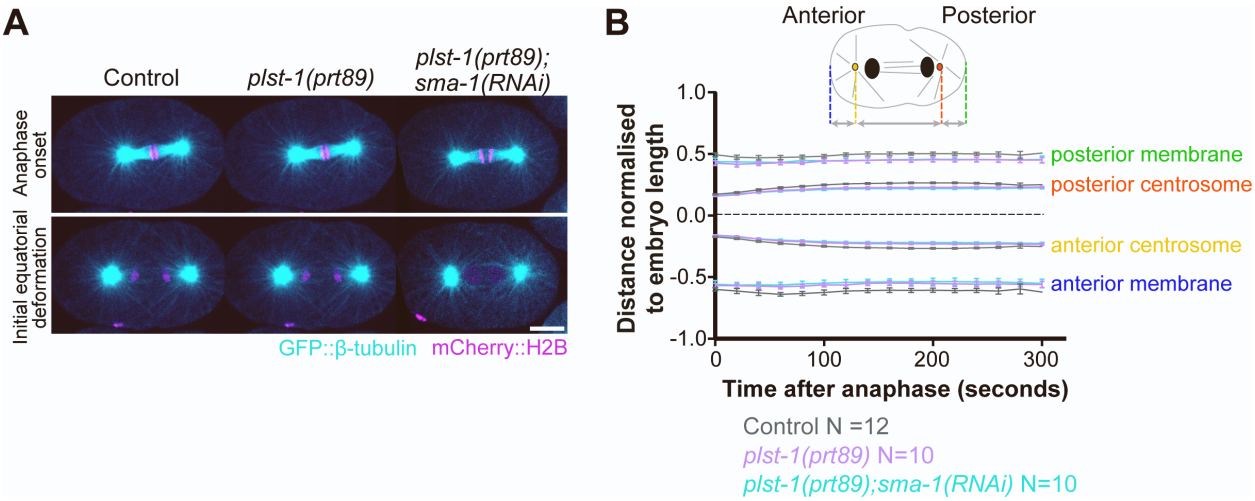

Figure S3. Mitotic spindle morphology and positioning is normal in *plst-1(prt89)* and *plst-1(prt89);sma-1(RNAi)* embryos. Related to Figure 5.

(A) Images of the central plane in one-cell embryos co-expressing GFP::β-tubulin and mCherry::histone H2B at anaphase onset and equatorial shallow deformation. Scale bar, 10 µm. **(B)** Centrosome positioning (mean ± 95% CI) along the anterior-posterior axis of the embryo over time after anaphase onset. Dashed line indicates the midpoint between the two centrosomes. N indicates the number of embryos analyzed.

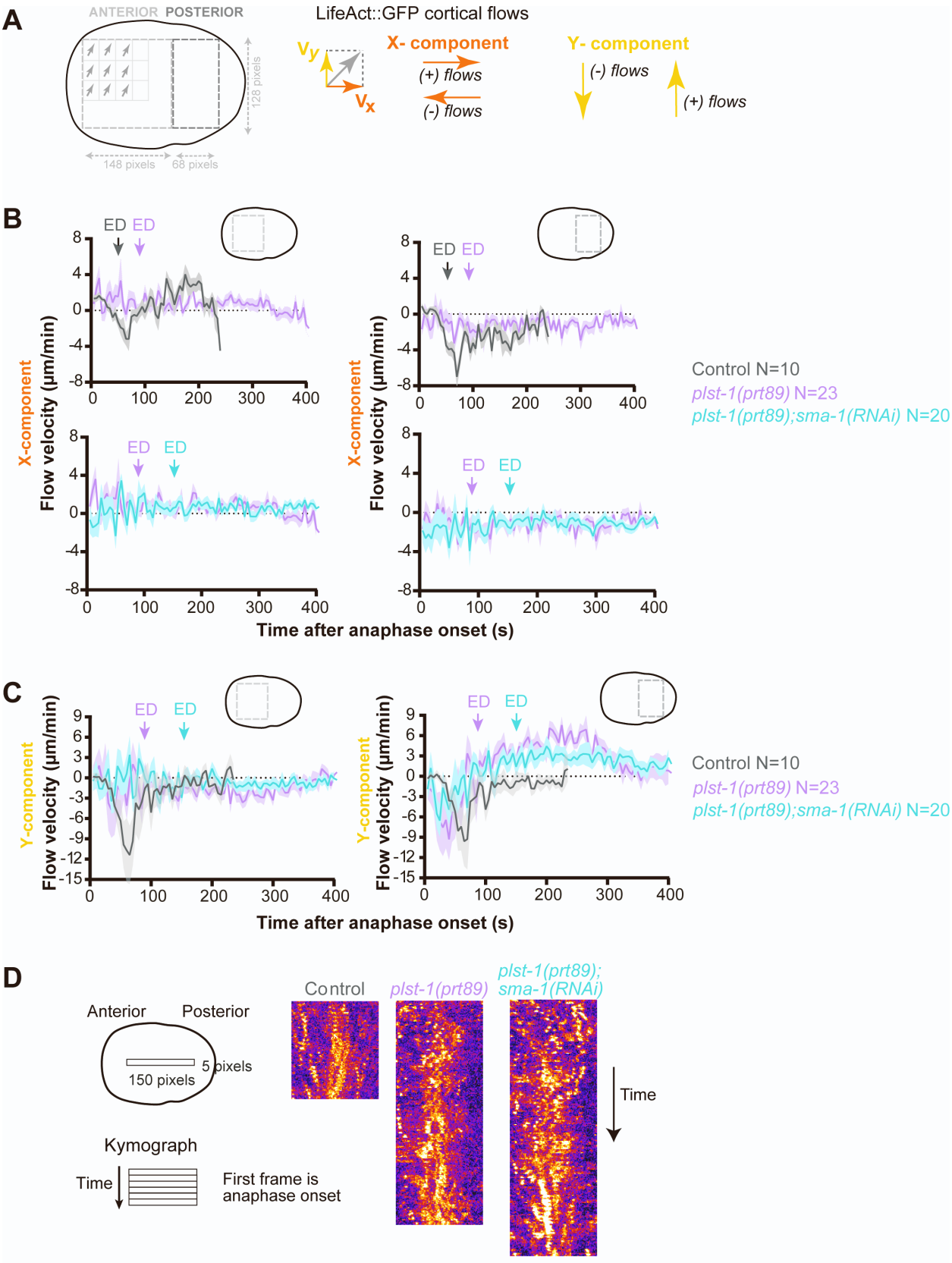
A
ANTERIOR POSTERIOR
128 pixels
148 pixels
68 pixels
LifeAct::GFP cortical flows
Vy
Vx
X- component
(+) flows
(-) flows
Y- component
(-) flows
(+) flows
B
ED ED
X-component
Flow velocity (µm/min)
Time after anaphase onset (s)
Control N=10
plst-1(prt89) N=23
plst-1(prt89);sma-1(RNAi) N=20
C
Y-component
Flow velocity (µm/min)
Time after anaphase onset (s)
Control N=10
plst-1(prt89) N=23
plst-1(prt89);sma-1(RNAi) N=20
D
Anterior
Posterior
5 pixels
150 pixels
Kymograph
Time
First frame is anaphase onset
Control
plst-1(prt89)
plst-1(prt89); sma-1(RNAi)
Time

Figure S4. Failure of cytokinesis in *plst-1(prt89);sma-1(RNAi)* embryos is not due to perturbed F-actin cortical flows. Related to Figure 5.

(A) Schematic illustrating the analysis of cortical F-actin flows by particle image velocimetry. X- and Y-components of the velocity vectors in the anterior or posterior regions of the embryo were averaged for each time point after anaphase onset. For the X-component, negative velocity values indicate posterior-anterior oriented flows and positive velocity values indicate anterior-posterior oriented flows. **(B,C)** X-component *(B)* or Y-component *(C)* flow velocities (mean ± SEM) at anterior *(left)* and posterior *(right)* cortex over time after anaphase onset in embryos expressing LifeAct::GFP. ED, initial equatorial deformation. Posterior-anterior directed flows in control embryos were particularly prominent on the posterior side, initiated before equatorial deformation, and peaked shortly thereafter (panel B, top right). F-actin cortical flows in *plst-1(prt89)* and *plst-1(prt89);sma-1(RNAi)* embryos were erratic and decreased in velocity (panel B, bottom right). N indicates the number of embryos analyzed. **(D)** Kymographs of the region indicated in the schematic on the left showing LifeAct::GFP cortical flows along the longitudinal axis in one-cell embryos, starting at anaphase onset.

A
Control
NMY-2::mCherry
LifeAct::GFP
sma-1(RNAi)
NMY-2::mCherry
LifeAct::GFP
plst-1(prt89)
NMY-2::mCherry
LifeAct::GFP
plst-1(prt89);sma-1(RNAi)
NMY-2::mCherry
LifeAct::GFP
50 s

Figure S5. Myosin coalescence into bright puncta in *plst-1(prt89);sma-1(RNAi)* embryos coincides with F-actin cluster formation. Related to Figures 5 and 6.

(A) Images of the equatorial cortical region in one-cell embryos co-expressing NMY-2::mCherry and LifeAct::GFP. First frame corresponds to the initial enrichment of NMY-2::mCherry at the cell equator. Scale bar, 10 μm.

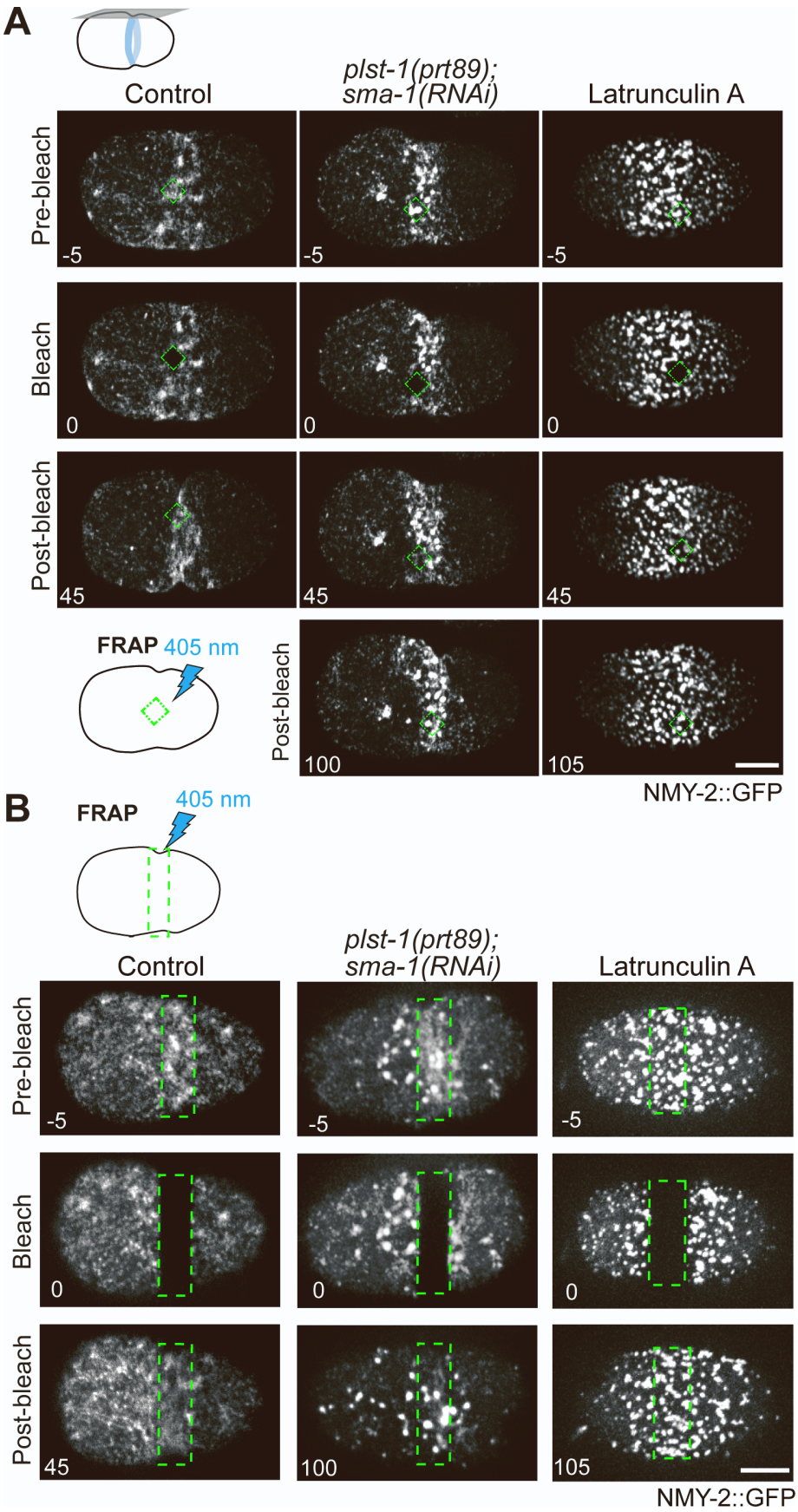
A
Control
plst-1(prt89); sma-1(RNAi)
Latrunculin A
Pre-bleach
Bleach
Post-bleach
-5
0
45
100
105
FRAP 405 nm
NMY-2::GFP
B
FRAP
405 nm
Control
plst-1(prt89); sma-1(RNAi)
Latrunculin A
Pre-bleach
Bleach
Post-bleach
-5
0
45
100
105
NMY-2::GFP

Figure S6. Fluorescence recovery after photobleaching of NMY-2::GFP at the cell equator. Related to Figure 6.

(A,B) Images of the cortex in *plst-1(prt89);sma-1(RNAi)* and Latrunculin A-treated one-cell embryos expressing NMY-2::GFP just before and after photobleaching of a portion *(A)* or the entire *(B)* cell equator at initial equatorial deformation, when myosin puncta start accumulating at the cell equator in *plst-1(prt89);sma-1(RNAi)* embryos. Numbers indicate the time in seconds relative to the photobleaching event. Schematics show the photobleached regions. Scale bars, 10 μm.

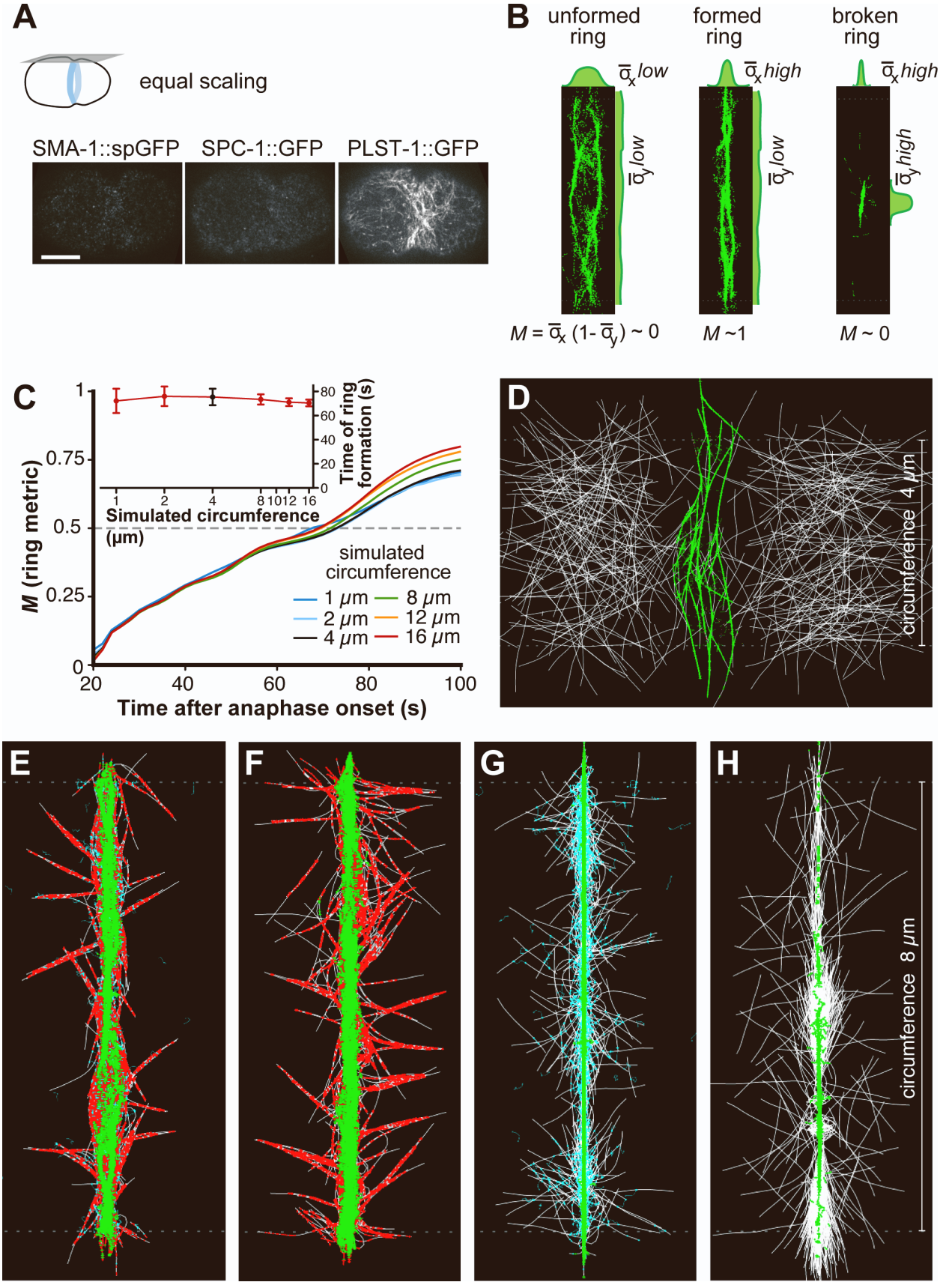
A
equal scaling
SMA-1::spGFP
SPC-1::GFP
PLST-1::GFP
B
unformed ring
formed ring
broken ring
$\bar{\sigma}_x$ low
$\bar{\sigma}_y$ low
$\bar{\sigma}_x$ high
$\bar{\sigma}_y$ low
$\bar{\sigma}_x$ high
$\bar{\sigma}_y$ high
$M = \bar{\sigma}_x (1 - \bar{\sigma}_y) \sim 0$
$M \sim 1$
$M \sim 0$
C
M (ring metric)
Time after anaphase onset (s)
Time of ring formation (s)
Simulated circumference (μm)
simulated circumference
1 μm
2 μm
4 μm
8 μm
12 μm
16 μm
D
circumference 4 μm
E
F
G
H
circumference 8 μm

Figure S7. Relative expression levels of GFP-tagged SMA-1 and PLST-1 in the early embryo, simulation metric calculation, and scaling and effects of no end-dwelling on depolymerizing ends. Related to Figures 3 and 7.

(A) Equally scaled images of the cortex in one-cell embryos expressing SMA-1::spGFP, SPC-1::GFP or PLST-1::GFP. Scale bar, 10 μm. **(B)** Simulation snapshots showing only myosin motors for simulations that (from left to right): fail to form a compact ring (double amount of plastin); successfully form a ring (reference simulation, same as last panel in Figure 7B); experience ring rupture (scenario with no plastins). Next to all snapshots are sketch plots that illustrate the measurements of x and y that are used for the ring metric (eq. 1). **(C)** Use of longer or shorter lengths of simulated circumference does not affect simulation results. Main plot: ring metric evolution for different circumference lengths. Inset: timing of ring formation or different circumference lengths ± SD. **(D)** Allowing motors to immediately fall off from depolymerizing barbed ends, instead of end-dwelling, leads to the gradual removal of F-actin from the ring midline and the ring forms with only a few F-actin fibers. **(E-H)** Simulation snapshots at 100 s after anaphase for scenarios with **(E)** all elements, **(F)** no spectrin, **(G)** no plastin, and **(H)** no plastin and no spectrin. Color legend: white - actin fibers, green - myosin, red - plastin, and cyan - βH/α-spectrin tetramer.

Fluorescent probe (expressed from transgene or endogenous locus; found in which strains)	**Method used for strain generation**	**Test of functionality**	**Reference**
LifeAct::GFP (transgene; GCP22, GCP927, GCP1163, GCP1164, GCP1169, GCP1170, GCP1176, GCP1187)	Bombardment	Normal cytokinesis timing in 1-cell embryo. Normal strain growth.	[S8]
LifeAct::RFP (transgene; GCP1207)	Bombardment	Normal cytokinesis timing in 1-cell embryo. Normal strain growth.	[S9]
PLST-1::GFP (endogenous locus; GCP831, GCP832, RZB217)	CRISPR/Cas9[a]	Normal cytokinesis timing in 1-cell embryo. Normal strain growth.	[S8]
NMY-2::GFP (endogenous locus; GCP113 and GCP570)	CRISPR/Cas9[a]	Normal cytokinesis timing in 1-cell embryo. Normal strain growth.	[S8]
NMY-2::mCherry (transgene; GCP22, GCP927, GCP1163, GCP1164, GCP1169, GCP1170, GCP1176, GCP1187)	MosSci[b], Chromosome II	NMY-2::mCherry is able to replace endogenous nmy-2. Normal strain growth.	[S10]
GFP::ANI-1 (transgene; OD130)	Bombardment	Normal strain growth. Pattern of localization of GFP::ANI-1 identical to that observed in strain MDX29, where the endogenous locus of ani-1 is tagged with mNeonGreen (Rehain-Bell et al., 2017).	[S11]
UNC-59::GFP (transgene; OD121)	Bombardment	UNC-59::GFP expression under the control of the pie-1 regulatory sequences	[S12]

		rescues the localization of UNC-61 (the other septin with which UNC-59 oligomerizes)	
SMA-1::splitGFP (endogenous locus; GCP991, GCP1207, GCP1208)	CRISPR/Cas9[a]	Normal strain growth.	This study
SPC-1::GFP (endogenous locus; GOU2936)	CRISPR/Cas9 [a]	Normal strain growth.	[S13]

[a] CRISPR/Cas9 - Clustered Regularly Interspaced Short Palindromic Repeats/CRISPR-associated protein 9

[b] MosSci - Mos1-mediated Single Copy Insertion

Table S1. Summary of fluorescent tagged proteins used in this study. Related to Figures 1-7.

Oligonucleotide purpose	**Oligonucleotide sequence (5'-3')**
For production of dsRNA against ani-1 (Y49E10.19)_Fwd	taatacgactcactataggTCAAACTCAATGGAGAGGACAA-3' *T7 promoter sequence is in lowercase*
For production of dsRNA against ani-1 (Y49E10.19)_Rev	aattaaccctcactaaaggCATTGTGCTTCAAATTCCTCAC *T3 promoter sequence is in lowercase*
For production of dsRNA against atn-1 (W04D2.1)_Fwd	aattaaccctcactaaaggCAAAAGCTCGAGGACTACCG *T3 promoter sequence is in lowercase*
For production of dsRNA against atn-1 (W04D2.1)_Rev	taatacgactcactataggAGCTGCGAATCTCTTCTTGG *T7 promoter sequence is in lowercase*
For production of dsRNA against fln-1 #1 (Y66H1B.2)_Fwd	aattaaccctcactaaaggCCGATTTCCAACTTCACTTCC *T3 promoter sequence is in lowercase*
For production of dsRNA against fln-1 #1 (Y66H1B.2)_Rev	taatacgactcactataggGACTTCACCAGCAACCTTAAC *T7 promoter sequence is in lowercase*
For production of dsRNA against fln-1 #2 (Y66H1B.2)_Fwd	aattaaccctcactaaaggTGGATGGGCAACTGTTTATG *T3 promoter sequence is in lowercase*
For production of dsRNA against fln-1 #2 (Y66H1B.2)_Rev	taatacgactcactataggGAGCTCCTCCTTCAGAGAAT *T7 promoter sequence is in lowercase*
For production of dsRNA against plst-1 (Y104H12BR.1)_Fwd	aattaaccctcactaaaggACTCGGAGTCCATGGAAATG *T3 promoter sequence is in lowercase*
For production of dsRNA against plst-1 (Y104H12BR.1)_Rev	taatacgactcactataggCACCATTTTTGGCTTCACCT *T7 promoter sequence is in lowercase*
For production of dsRNA against unc-59 (W09C5.2)_Fwd	taatacgactcactataggCGTGAAACTCGTGGAGAACA *T7 promoter sequence is in lowercase*
For production of dsRNA against unc-59 (W09C5.2)_Rev	aattaaccctcactaaaggTTGTGGTGGAGTTCAACGTG *T3 promoter sequence is in lowercase*
For production of dsRNA against unc-61 (Y50E8A.4)_Fwd	taatacgactcactataggAGCTGTCGAAGCTGGATTTC *T7 promoter sequence is in lowercase*
For production of dsRNA against unc-61 (Y50E8A.4)_Rev	aattaaccctcactaaaggACGGCTGAACTCGTCTTGAT *T3 promoter sequence is in lowercase*
For production of dsRNA against unc-70 (K11C4.3)_Fwd	aattaaccctcactaaaggCACTGTCTTGAGAACGTTGAG *T3 promoter sequence is in lowercase*

For production of dsRNA against unc-70 (K11C4.3)_Rev	taatacgactcactataggAATGGATTTCTCATCAGGTTGG *T7 promoter sequence is in lowercase*
For production of dsRNA against erm-1 (C01G8.5)_Fwd	aattaaccctcactaaaggCTTCTACGCTCCACGACTCC *T3 promoter sequence is in lowercase*
For production of dsRNA against erm-1 (C01G8.5)_Rev	taatacgactcactataggCTCCATATGCAGAACGTCGTA *T7 promoter sequence is in lowercase*
Single guide RNA #1 used to generate *sma-1*ΔABD#1 mutant	TCACGCATTCGGACACTGC
Single guide RNA #2 used to generate *sma-1*ΔABD#1 mutant	GTGCAACTCCTTTCTTAAT
Single guide RNA #3 used to generate *sma-1*ΔABD#1 mutant	ATTGACTTCTCGTCAGGCC
Repair template used to generate *sma-1*ΔABD#1 mutant	cagGTTCGTGTTCCAACAAGTGGTGCACCACCAGTTCG CGCAGATGCCAATGGAACAGATCA**G**GACGAGTTCAA TAATGAGACACTGTACTTTGAAAGATCACGCATTCGG ACACTGCA**A**GACGAACGTGTGAAGCAAAAGACTGAG ATGACAGGAGCTCGACGTATTGCTAATgtaagtgtttataagtt catg *in bold are silent mutations introduced to avoid repair template recognition by Cas9 or to maintain codon balance; bases in lowercase indicate intron regions*
For screening of *sma-1*ΔABD#1 successful events_Fwd	GGAAAGACGCTGAGCTAGTA
For screening of *sma-1*ΔABD#1 successful events_Rev	CTCCTTGTACTTTGGTGGTTTC
crRNA #1 used to generate *sma-1*ΔABD#2 mutant	CTCGTCTTGATCTGTTCCAT
crRNA #2 used to generate *sma-1*ΔABD#2 mutant	TTAAATTTTTCAGGATGAGG
Repair template used to generate *sma-1*ΔABD#2 mutant	aaagttttaaagatccgaaaaaaaactgagaacgtttagaaatatttaacagttcaattagc atcaagttcataatgatttttttcagGTTCGTGTTCCAACAAGTGGTGC ACCACCAGTTAATCGG-intron3/4- GATGAGGAAGAGCGTGGAGAGCGAAAACATGCCAA AGATGCCTTGCTGTTGTGGTGTCAGAGAAAAACAGC TGGATATCCAAATGTTCGCATCGAGAACTTCACTACA AGTTGG *bases in lowercase indicate intron regions; intron3/4 as in sma-1 transcript R31.1a, Wormbase version WS279*
For screening of *sma-1*ΔABD#2 successful events_Fwd	AACGGAAAGACGCTGAGCTAGT

For screening of *sma-1*ΔABD#2 successful events_Rev	GATCCGGACGGTGCGAATGG
crRNA #1 used to generate *sma-1*ΔSH3 mutant	ATTGACTGGTAGTAGCAGTG
crRNA #2 used to generate *sma-1*ΔSH3 mutant	TCTAGACTGACCATGACCTT
Repair template used to generate *sma-1*ΔSH3 mutant	gcagGAGTGACATCAGTCGACTCGAGGAGATGCAAAG TCAGCTAGCAAACGAAGGTCATGGTCAGTCTAGAAA AATCGAAGTTCGTCAACATAAGATCAA *bases in lowercase indicate intron regions*
For screening of *sma-1*ΔSH3 successful events_Fwd	CAGTCGACTCGAGGAGATGC
For screening of *sma-1*ΔSH3 successful events_Rev	TGGTTTCAAATCACGCTCCA
Single guide RNA #1 used to generate *sma-1*ΔPH mutant	TGGGTGCTATTGACATGAA
Single guide RNA #2 used to generate *sma-1*ΔPH mutant	ACGACTTGAGCTGATTACT
Repair template used to generate *sma-1*ΔPH mutant	CGTTCAATACTCGTCGTACTCAATCAATCCGCAAAGG AAGTCGCTGGGAAGATATGGGTCCA**TCCAA**TCA**ACT GAAATC**GTATGCGTACAACGgttagttaattactatttaaattattaacc agtttgcttctcag *in bold are silent mutations introduced to avoid repair template recognition by Cas9 or to maintain codon balance*
For screening of *sma-1*ΔPH successful events_Fwd	GCAAAGACTACCGCTGATTT
For screening of *sma-1*ΔPH successful events_Rev	GTTGATCTGGACTTTGGAAGAG
Single guide RNA #1 used to generate *sma-1*Δ11SR mutant	CGTGACCTCGGTCGAGATGT
Single guide RNA #2 used to generate *sma-1*Δ11SR mutant	TTACAAGATAAGGAAGCGAC
Repair template used to generate *sma-1*Δ11SR mutant	GTGACGTTGACGAGTTTGAGCAATGGATGGCAGACA AAATGGCCAACATGGTAGCAATGGAACAGGAAGATC TTTCGAGAGCTGATCTTGCTTCCGTGAA
For screening of *sma-1*Δ11SR successful events_Fwd	AGCAGGAAGCACTCAGAACC
For screening of *sma-1*Δ11SR successful events_Rev	GCCGAGTATCTGGGAACGAG

Single guide RNA #1 used to generate *atn-1*ΔABD mutant	AGGACTGTTAGATCCAGCA
Single guide RNA #2 used to generate *atn-1*ΔABD mutant	GGACTGTTAGATCCAGCAT
Single guide RNA #3 used to generate *atn-1*ΔABD mutant	ATGCTGGATCTAACAGTCC
Repair template used to generate *atn-1*ΔABD mutant	CATACCATCAGCCGGGCTACGACTACACTCAACAAG AGGAAGAATGGGACCGTGAAGGA**TTACTG**GATCC**T** GC**C**TGGGAGGCATT**T**CGTAACATGCGTGATCCTCCAC CACCAGTTATTCGCCAACCACCACCACAGCGTGTTGT TGTTGCTCCACCTCCAGAG *in bold are silent mutations introduced to avoid repair template recognition by Cas9 or to maintain codon balance*
For screening of *atn-1*ΔABD successful events_Fwd	CCTTCTTCACACCGTTCATC
For screening of *atn-1*ΔABD successful events_Rev	GAGACAAGGACAATGGACATTTA
Single guide RNA #1 used to generate *sma-1::spGFP*	TCGGATCGTTATTCAAGCG
Single guide RNA #2 used to generate *sma-1::spGFP*	GGTATCTACTTTGAATGTT
Single guide RNA #3 used to generate *sma-1::spGFP*	TGAAGATCAGCGTGTGGTG
For screening of *sma-1::spGFP* successful events_Fwd	GCGAATTCATTACTTGGGTAGA
For screening of *sma-1::spGFP* successful events_Rev	GTCTTCCAGCTTTGGTGATAG
Single guide RNA used to generate *plst-1::mCherry*	CCATTAATCATCGGAACAAT
For screening of *plst-1::mCherry* successful events_Fwd	GGTGGCATGGATGAATTG
For screening of *plst-1::mCherry* successful events_Rev	CCAAATTTAGGCTAGAAACTCGAT

Table S2. List of oligonucleotides used in this study. Related to Figures 1-4 and 7.

Parameter	Symbol	Value Range (standard value)
Actin Rigidity	μ_{actin}	0.075 pN μm^2 [S14]
Actin Segmentation Length	l_{actin}	0.1 μm
Actin Fiber Length (initial)	L_{actin}	1 μm [S15]
Growing Speed of Barbed End	v_{b+}	0 - 0.8 μm/s (0.08 μm/s) [S16]
Shrinking Speed of Barbed End	v_{b-}	0 - 0.56 μm/s (0.056 μm/s) [S16]
Growing Speed of Pointed End	v_{p+}	0 μm/s
Shrinking Speed of Pointed End	v_{p-}	0 - 0.14, μm/s (.014 μm/s) [S16]
Switch Rate to Depolymerization	r_c	8 Hz
Switch Rate to Polymerization	r_r	4 Hz
Backbone Length of Myosin	L_{motor}	0.15 μm [S17]
Number of Binding Heads of Myosin	n	8
Binding Range of Motor Head	d_{bind}	0.01 μm
Binding Rate of Motor Head	b_{motor}	10 Hz [S18]
Unbinding Rate of Motor Head	u_{motor}	0.3 Hz [S18]
Maximum Motor Speed	v_0	0.1 μm/s [S19]
Stall Force	f_0	4 pN [S20]
Backbone Resting Length of Plastin	$l_{plastin}$	0.012 μm [S21]
Spring Stiffness	k	250 pN/μm
Binding Range of Plastin	d_{bind}	0.01 μm
Binding Rate of Plastin	$b_{plastin}$	10 Hz
Unbinding Rate of Plastin	$u_{plastin}$	0.5 Hz
Maximum Allowed Angular Difference	$\Delta\theta_{max}$	10 degrees
Rescue Probability of Plastin	$r_{plastin}$	0.1

βH-Spectrin Rigidity	$\mu_{spectrin}$	$7.5*10^{-5}$ pN μm^2 [S22]
βH-Spectrin Segmentation Length	$l_{spectrin}$	0.05 μm
βH-Spectrin Backbone Length	$L_{spectrin}$	0.15-0.35 μm (0.2 μm)
Binding Range of Binding Head	d_{bind}	0.01 μm
Binding Rate of Binding Head	$b_{spectrin}$	10 Hz
Unbinding Rate of Binding Head	$u_{spectrin}$	0.5 Hz
Rescue Probability of βH-Spectrin	$r_{spectrin}$	0.1
Width (Non Periodic Boundary)	x_0	10 μm
Height (Periodic Boundary)	y_0	1-16 μm (4 μm)
Initial Component Horizontal Range	x_i	3 μm
Background Viscosity	ν	1 pN s / μm^2 [S23]
Background Temperature	kT	0.0042 pN μm
Fiber Count	N_F	94-1,500 (375)
Motor Count	N_M	260-4,168 (1,042)
Plastin Count	N_P	0-120,000 (30,000)
βH-spectrin Count	N_S	0-5,600 (1,400)

Table S3. Cytosim parameters used in simulations (where parameters were varied, base values are shown in parentheses). Related to Figures 7 and S7.

Supplemental References

S1. Moorthy, S., Chen, L., and Bennett, V. (2000). Caenorhabditis elegans beta-G spectrin is dispensable for establishment of epithelial polarity, but essential for muscular and neuronal function. J. Cell Biol. *149*, 915–930.

S2. Chan, F.-Y., Silva, A.M., Saramago, J., Pereira-Sousa, J., Brighton, H.E., Pereira, M., Oegema, K., Gassmann, R., and Carvalho, A.X. (2019). The ARP2/3 complex prevents excessive formin activity during cytokinesis. Mol. Biol. Cell *30*, 96–107.

S3. Kovacevic, I., and Cram, E.J. (2010). FLN-1/filamin is required for maintenance of actin and exit of fertilized oocytes from the spermatheca in C. elegans. Dev. Biol. *347*, 247–257.

S4. Maddox, A.S., Habermann, B., Desai, A., and Oegema, K. (2005). Distinct roles for two C. elegans anillins in the gonad and early embryo. Development *132*, 2837–2848.

S5. Moulder, G.L., Cremona, G.H., Duerr, J., Stirman, J.N., Fields, S.D., Martin, W., Qadota, H., Benian, G.M., Lu, H., and Barstead, R.J. (2010). α-actinin is required for the proper assembly of Z-disk/focal-adhesion-like structures and for efficient locomotion in Caenorhabditis elegans. J. Mol. Biol. *403*, 516–528.

S6. Ono, S. (2001). The Caenorhabditis elegans unc-78 gene encodes a homologue of actin-interacting protein 1 required for organized assembly of muscle actin filaments. J. Cell Biol. *152*, 1313–1319.

S7. Maddox, A.S., Lewellyn, L., Desai, A., and Oegema, K. (2007). Anillin and the septins promote asymmetric ingression of the cytokinetic furrow. Dev. Cell *12*, 827–835.

S8. Leite, J., Chan, F.-Y., Osório, D.S., Saramago, J., Sobral, A.F., Silva, A.M., Gassmann, R., and Carvalho, A.X. (2020). Equatorial Non-muscle Myosin II and Plastin Cooperate to Align and Compact F-actin Bundles in the Cytokinetic Ring. Front Cell Dev Biol *8*, 573393.

S9. Ding, W.Y., Ong, H.T., Hara, Y., Wongsantichon, J., Toyama, Y., Robinson, R.C., Nédélec, F., and Zaidel-Bar, R. (2017). Plastin increases cortical connectivity to facilitate robust polarization and timely cytokinesis. J. Cell Biol. *216*, 1371–1386.

S10. Osório, D.S., Chan, F.-Y., Saramago, J., Leite, J., Silva, A.M., Sobral, A.F., Gassmann, R., and Carvalho, A.X. (2019). Crosslinking activity of non-muscle myosin II is not sufficient for embryonic cytokinesis in C. elegans. Development *146*.

S11. Lewellyn, L., Carvalho, A., Desai, A., Maddox, A.S., and Oegema, K. (2011). The chromosomal passenger complex and centralspindlin independently contribute to contractile ring assembly. J. Cell Biol. *193*, 155–169.

S12. Carvalho, A., Desai, A., and Oegema, K. (2009). Structural memory in the contractile ring makes the duration of cytokinesis independent of cell size. Cell *137*, 926–937.

S13. Jia, R., Li, D., Li, M., Chai, Y., Liu, Y., Xie, Z., Shao, W., Xie, C., Li, L., Huang, X., et al. (2019). Spectrin-based membrane skeleton supports ciliogenesis. PLoS Biol. *17*, e3000369.

S14. Gittes, F., Mickey, B., Nettleton, J., and Howard, J. (1993). Flexural rigidity of microtubules and actin filaments measured from thermal fluctuations in shape. J. Cell Biol. *120*, 923–934.

S15. Burlacu, S., Janmey, P.A., and Borejdo, J. (1992). Distribution of actin filament lengths measured by fluorescence microscopy. American Journal of Physiology-Cell Physiology *262*, C569–C577.

S16. Shekhar, S., and Carlier, M.-F. (2017). Enhanced depolymerization of actin filaments by ADF/Cofilin and monomer funneling by capping protein cooperate to accelerate barbed-end growth. Curr. Biol. *27*, 1990–1998.e5.

S17. Billington, N., Wang, A., Mao, J., Adelstein, R.S., and Sellers, J.R. (2013). Characterization of three full-length human nonmuscle myosin II paralogs. J. Biol. Chem. *288*, 33398–33410.

S18. Guo, B., and Guilford, W.H. (2006). Mechanics of actomyosin bonds in different nucleotide states are tuned to muscle contraction. Proc. Natl. Acad. Sci. U. S. A. *103*, 9844–9849.

S19. Barua, B., Nagy, A., Sellers, J.R., and Hitchcock-DeGregori, S.E. (2014). Regulation of nonmuscle myosin II by tropomyosin. Biochemistry *53*, 4015–4024.

S20. Walcott, S., Warshaw, D.M., and Debold, E.P. (2012). Mechanical coupling between myosin molecules causes differences between ensemble and single-molecule measurements. Biophys. J. *103*, 501–510.

S21. Matsudaira, P., Mandelkow, E., Renner, W., Hesterberg, L.K., and Weber, K. (1983). Role of fimbrin and villin in determining the interfilament distances of actin bundles. Nature *301*, 209–214.

S22. Stokke, B.T., Mikkelsen, A., and Elgsaeter, A. (1985). Human erythrocyte spectrin dimer intrinsic viscosity: temperature dependence and implications for the molecular basis of the erythrocyte membrane free energy. Biochim. Biophys. Acta *816*, 102–110.

S23. Daniels, B.R., Masi, B.C., and Wirtz, D. (2006). Probing single-cell micromechanics in vivo: the microrheology of C. elegans developing embryos. Biophys. J. *90*, 4712–4719.